

Čerenkov free-electron laser in side-wall configuration

Yashvir Kalkal* and Vinit Kumar†

Homi Bhabha National Institute, Mumbai 400094, India

Accelerator and Beam Physics Laboratory,

Raja Ramanna Centre for Advanced Technology, Indore 452013, India

Abstract

We have proposed a Čerenkov free-electron laser (CFEL) with metallic side walls. In this system, metallic side walls are used to confine the surface mode supported by a thin dielectric slab placed at the top of a conducting surface. This leads to an enhancement in the coupling between the optical mode and the co-propagating electron beam, and consequently, the performance of CFEL is improved. We set up coupled Maxwell-Lorentz equations for the system, in analogy with the undulator based conventional FELs; and obtain formulas for small signal gain and growth rate. It has been shown that the small signal gain and the growth rate in the sidewall configuration of CFEL are larger compared to the configuration without side walls. In the nonlinear regime, we solve the coupled Maxwell-Lorentz equations numerically and study the saturation behaviour of the system. It is found that the Čerenkov FEL with side walls attains saturation quickly, and produces powerful coherent terahertz (THz) radiation.

PACS numbers: 41.60.Bq, 41.60.Cr, 42.82.Et

* yashvirkalkal@gmail.com

† vinit@rrcat.gov.in

I. INTRODUCTION

During recent times, terahertz (THz) radiation is widely used to investigate the spectral signatures of biological and chemical molecules, and in imaging and security related applications [1]. Čerenkov free-electron laser (CFEL), which uses a low energy electron beam is seen as a compact source of tunable, high power coherent THz radiation [2–9]. In the basic configuration of a CFEL, a dielectric slab placed on an ideal conductor supports an electromagnetic surface mode. Under suitable conditions, the surface mode can interact with the co-propagating electron beam to produce coherent electromagnetic radiation.

In most of the earlier analyses, the working of CFELs has been discussed by neglecting the three dimensional (3D) effects, i.e., the effects due to variation of the electromagnetic field in surface mode in the direction perpendicular to the electron beam, and parallel to the plane of dielectric surface [2–4]. Andrew and Brau [5] proposed a 3D theory of CFELs by using hydrodynamic approach, and showed that the gain reduces significantly due to the diffraction of the surface mode. Recently, we have derived Maxwell-Lorentz equations to analyze the working of CFELs driven by a flat electron beam in both linear and non-linear regime [6], and extended our analysis to include the 3D effects [7]. Including the 3D effects due to diffraction, the small-signal gain of a CFEL driven by a flat beam is shown to be proportional to the effective surface current density $K = I/\Delta y_e$, where I is the beam current and $\Delta y_e = \sqrt{\pi\beta_p\lambda L/4}$ [7] is the effective mode width, $\beta_p = v_p/c$, v_p is phase velocity of the surface mode, c is the speed of light, λ is the free space wavelength and L is length of the dielectric slab. For a given value of β_p and λ , the effective mode width described above is the minimum possible value, which is limited by diffraction, and this can be reduced only if L is reduced. The small-signal gain has a cubic dependence on the length L , and therefore, we would like to increase L to increase the value of gain. However, as we increase the value of L to get a reasonable value of gain, the value of Δy_e increases, which reduces the gain. The question therefore arises whether we can reduce the effective mode width below the value described above, and make it independent of L . It turns out that this can be achieved using waveguiding, as it is done in conventional FELs. This helps in increasing the gain, and thus achieving a reasonable value of gain in shorter interaction length.

The surface mode supported in a CFEL is evanescent in the direction perpendicular to the dielectric surface with scale height $h = \beta_p\gamma_p\lambda/4\pi$ [7], where $\gamma_p = 1/\sqrt{1 - \beta_p^2}$. To maintain a

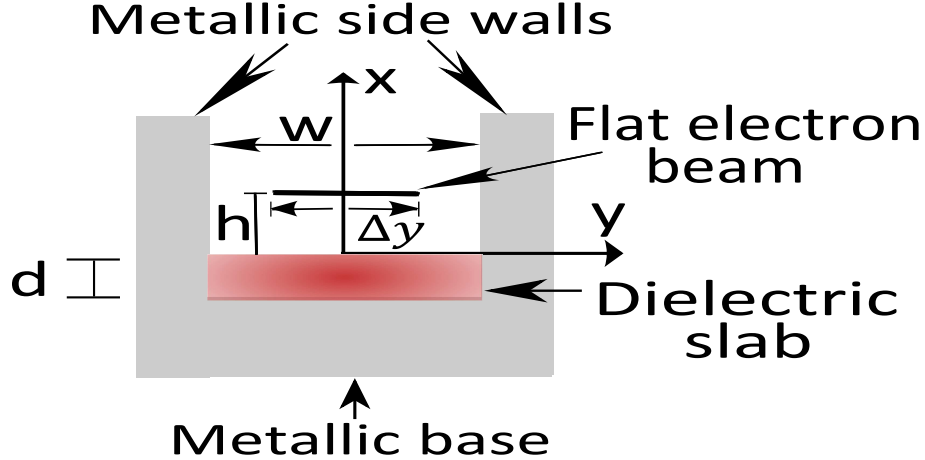


FIG. 1. Schematic of a Čerenkov FEL with metallic side walls.

good overlap with the radiation beam, the electron beam has to maintain its vertical beam size around this value over the entire interaction length. As discussed in Refs. [6, 7], one of the challenges in a CFEL is to maintain a very small vertical beam size over the entire interaction length. With the help of waveguiding, the requirement of interaction length is reduced, and therefore, we need to maintain small vertical beam size now over a *smaller* interaction length, which relaxes the requirement on vertical beam emittance. Further, the attenuation of the surface mode due to finite conductivity of the metal can also reduce the gain of a CFEL system [7]. However, in case of waveguiding, we can take shorter interaction length as discussed earlier, and can minimize the attenuation effects such that the device can produce powerful electromagnetic radiation.

The waveguiding in CFELs can be achieved by having metallic side walls along the dielectric slab as shown in Fig. 1. The separation between the side walls w is taken as width of the dielectric slab. Due to the presence of metallic side walls, the surface mode is guided and maintains a constant width over any arbitrary length. Smaller value of mode width results in a good overlapping between the electron beam and the copropagating guided surface mode; and consequently the gain of CFEL can be increased. We would like to mention that the concept of side walls has been introduced earlier in the Smith-Purcell free-electron laser (SP-FEL) and side wall grating structure is found to be advantageous compared to the general grating (without side walls) [10–12]. We expect similar improvement for the CFELs.

In this paper, we present a detailed analysis of CFEL in sidewall configuration. In next

section, we will derive the dispersion relation for the CFEL with side walls, and derive the coupled Maxwell-Lorentz equations for the system. We also discuss the analytical calculations of small-signal gain and growth rate in the linear regime, and the numerical solution of the coupled Maxwell-Lorentz equations in the non-linear regime, in the next section. In Appendix A, we set up the field equations for the surface mode supported in the empty structure (without electron beam) of a side wall CFEL, and perform the calculations for the power, group velocity, and the attenuation coefficient of the surface mode.

II. THEORY AND CALCULATIONS

A. Formula for wavelength

The schematic of Čerenkov FEL with side walls is shown in Fig. 1. A dielectric slab with thickness d , length L , and relative dielectric permittivity ϵ is placed on a metallic surface. In the y -direction, dielectric slab is surrounded with metallic side walls with spacing w . A flat electron beam of width Δy in the y -direction, having vanishing thickness in the x -direction, is propagating with velocity v along the z -direction at a height h above the dielectric surface. The electromagnetic surface mode supported by this geometry can be obtained by combining the plane wave solutions of an open structure, i.e., the structure without any side walls, in a suitable manner such that it satisfies the boundary conditions. Field components of the lowest order TM surface mode, which satisfy the Maxwell equations with the given boundary conditions are discussed in detail in Appendix A. The expression for E_z^I is given by,

$$\begin{aligned} E_z^I &= E_0 e^{-\Gamma(x-h)} e^{i(k_z z - \omega t)} \cos(k_y y) + \text{c.c.}, \\ &= \frac{E_0}{2} [e^{i(k_z z + k_y y - \omega t)} + e^{i(k_z z - k_y y - \omega t)}] e^{-\Gamma(x-h)} + \text{c.c.} \end{aligned} \quad (1)$$

Here, E_0 is the peak amplitude of E_z^I at the location of the electron beam at $x = h$, $k_z = 2\pi/\beta\lambda$ is the propagation wavenumber in the z -direction, $\beta = v/c$, $\omega = 2\pi c/\lambda$, $\Gamma = \sqrt{k_y^2 + k_z^2 - \omega^2/c^2}$ and $k_y = \pi/w$ for the lowest order mode. The phase velocity is here taken as equal to the electron velocity. As it is seen in the above equation, the guided surface mode is a combination of two plane waves, each having frequency ω and wave vector $k_0 = \sqrt{k_y^2 + k_z^2}$, and travelling in different directions in the (y, z) plane. Each of these two plane waves is a solution of the wave equation for the case of CFEL without side walls, and should therefore satisfy the corresponding dispersion relation $k_0 = \tan^{-1}(1/a)/b$ for that case [6]

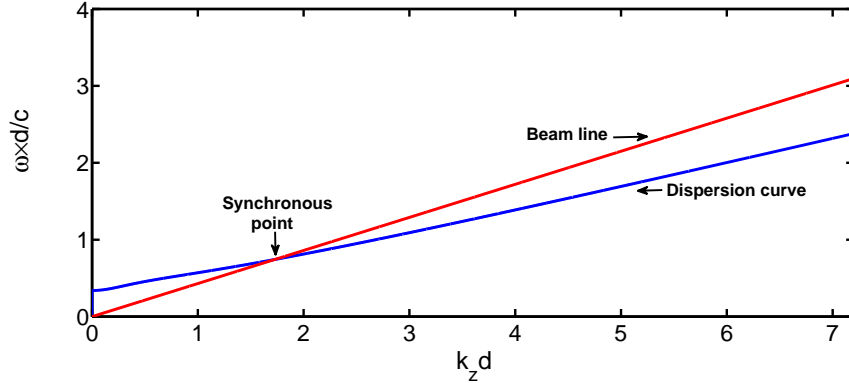


FIG. 2. Plot of the dispersion curve of the electromagnetic surface mode, and the Doppler line for the electron beam. The resonant frequency of the CFEL system is obtained at the intersection.

. Here, $a = (\gamma_p/\epsilon)\sqrt{\epsilon\beta_p^2 - 1}$, $b = d\sqrt{\epsilon\beta_p^2 - 1}$, and $\beta_p = \omega/ck_0$. Note that here we have used the property that the dielectric slab is an isotropic structure in the (y, z) plane. Using this dispersion relation, we obtain the following expression for the operating wavelength of a sidewall CFEL:

$$\lambda = \frac{2\pi}{\beta\sqrt{[\tan^{-1}(1/a)/b]^2 - [\pi/w]^2}}. \quad (2)$$

From the above equation, it is clear that for a finite sidewall spacing w , we typically require an electron beam with higher energy to achieve the same operating wavelength, as compared to the case of CFEL without any side walls, provided that all other parameters are same. The dispersion curve for a CFEL with side walls is shown in Fig. 2. The parameters used in our calculations are summarized in Table 1. For the dielectric slab, we choose sapphire material with relative dielectric permittivity $\epsilon = 9.6$. As discussed in detail in the next section, we have taken side wall spacing $w = (2/5)\sqrt{\pi\beta_p\lambda L/4}$, which gives an enhancement in small signal gain up to a factor of five, compared to the case of CFEL without any side walls. The resonant frequency is obtained as 0.11 THz for these parameters.

B. Analytical calculations of gain and growth rate

Next, we will derive the coupled Maxwell-Lorentz equations to study the interaction of the guided surface mode with the co-propagating electron beam in a sidewall CFEL. Here, we have adopted a model given in Ref. [13] which is very successful for the detailed analysis of

backward wave oscillators (BWOs) based on corrugated waveguide geometry. In this model, an ensemble of electrons interact with the co-propagating surface mode, and the amplitude $A(z, t)$ of the surface mode is a slowly varying function of z and t , due to interaction with the co-propagating electron beam. Now, the electromagnetic surface field described earlier in the section can be written in a more general form as

$$\mathbf{E}^T = [A(z, t)\mathbf{E}_p(\mathbf{x}, \mathbf{k}_y) + \mathbf{E}_{sc}]e^{i(k_z z - \omega t)} + c.c., \quad (3)$$

$$\mathbf{B}^T = [A(z, t)\mathbf{B}_p(\mathbf{x}, \mathbf{k}_y) + \mathbf{B}_{sc}]e^{i(k_z z - \omega t)} + c.c.. \quad (4)$$

Here, the symbols \mathbf{E}_p and \mathbf{B}_p are used to denote the complex amplitude of the field components which represent the solutions of the electromagnetic fields in the empty structure, i.e., in the absence of electron beam. The components of \mathbf{E}_p and \mathbf{B}_p in x, y and z directions are written explicitly in the Appendix A. The terms \mathbf{E}_{sc} and \mathbf{B}_{sc} denote the small first-order space charge fields. The total electromagnetic field will satisfy Maxwell equations with the beam current density \mathbf{J} to give:

$$\begin{aligned} \frac{1}{c^2} \frac{\partial A}{\partial t} \mathbf{E}_p - \frac{i\omega}{c^2} \mathbf{E}_{sc} &= \nabla \times \mathbf{B}_{sc} + ik_z \hat{z} \times \mathbf{B}_{sc} \\ &+ \frac{\partial A}{\partial z} \hat{z} \times \mathbf{B}_p - \mu_0 \mathbf{J} e^{-i(k_z z - \omega t)}, \end{aligned} \quad (5)$$

$$\begin{aligned} -\frac{\partial A}{\partial t} \mathbf{B}_p + i\omega \mathbf{B}_{sc} &= \nabla \times \mathbf{E}_{sc} + ik_z \hat{z} \times \mathbf{E}_{sc} \\ &+ \frac{\partial A}{\partial z} \hat{z} \times \mathbf{E}_p, \end{aligned} \quad (6)$$

TABLE I. Parameters of a sidewall CFEL used in the calculation

| | |
|------------------------------------|-------------------|
| Electron energy | 55 keV |
| Electron-beam height (h) | 100 μm |
| Electron-beam current (I) | 35 mA |
| Dielectric constant (ϵ) | 9.6 |
| Length of slab (L) | 5 cm |
| Dielectric thickness (d) | 320 μm |
| Side walls separation (w) | 2.7 mm |
| Operating frequency | 0.11 THz |

where, μ_0 is the permeability of the free space. By taking the dot product of Eq. (5) with \mathbf{E}_p^* , and Eq. (6) with \mathbf{B}_p^* , and subtracting the resultants, respectively; we obtain:

$$\left[\frac{|\mathbf{E}_p|^2}{c^2} + |\mathbf{B}_p|^2 \right] \frac{\partial A}{\partial t} + \hat{z} \cdot [\mathbf{E}_p^* \times \mathbf{B}_p + \mathbf{E}_p \times \mathbf{B}_p^*] \frac{\partial A}{\partial z} = -\mu_0 \mathbf{J} \cdot \mathbf{E}_p^* e^{-i(k_z z - \omega t)} + \nabla \cdot [\mathbf{B}_{sc} \times \mathbf{E}_p^* - \mathbf{E}_{sc} \times \mathbf{B}_p^*]. \quad (7)$$

Here, the fact that both \mathbf{E}_p^* and \mathbf{B}_p^* satisfy free-space wave equation have been used to derive above equation. We performed integration on both sides of Eq. (7) for x in the range $(0, \infty)$, and y in the range $(-w/2, +w/2)$. The last term on the right hand side of Eq. (7) will vanish upon integration, and we obtain:

$$\frac{\partial A}{\partial t} + v_g \frac{\partial A}{\partial z} = -\frac{|A|^2}{U'w} \int_{-w/2}^{w/2} \int_0^\infty \mathbf{J} \cdot \mathbf{E}_p^* e^{-i(k_z z - \omega t)} dx dy dz, \quad (8)$$

where, v_g is group velocity of the surface mode, which is equal to $P/U'w$ for the CFEL [6], P is total power contained in the electromagnetic surface mode, and U' is the electromagnetic energy stored in the field per unit length L per unit mode width w . The current density of the flat beam propagating at height h from the dielectric surface is given by $\mathbf{J} = (I/\Delta y)\delta(x-h)\hat{z}$, where I is the beam current and Δy is the width of the electron beam. The z component of the electromagnetic field \mathbf{E}_p , which interacts with the electron beam is given by $E_0 \cos(k_y y) e^{-\Gamma(x-h)} \hat{z}$, and the term AE_o is represented by E_z in further calculations. Substituting \mathbf{E}_p^* and \mathbf{J} in Eq. (8) and performing the integral, we obtain the following time dependent differential equation for E_z :

$$\frac{\partial E_z}{\partial z} + \frac{1}{v_g} \frac{\partial E_z}{\partial t} = -\frac{I \langle e^{-i\psi} \rangle}{v_g w U' / E_z^2} \left(\frac{\sin(k_y \Delta y / 2)}{k_y \Delta y / 2} \right). \quad (9)$$

Here, $\langle \dots \rangle$ represents averaging over total number of electrons distributed over one wavelength of the evanescent field, the term $\langle e^{-i\psi} \rangle$ represents bunching factor which arises due to interaction of the electron beam with the co-propagating surface mode, and $\psi = k_z z - \omega t$ is phase of electron. Due to the interaction between the surface mode and the electron beam, electrons get bunched at the resonant frequency ω of the surface mode. Next, we take the effect of attenuation of the surface mode due to the ohmic losses present on the surface of conductor and due to the losses present in the dielectric medium. In the presence of losses, the surface wave will attenuate as it propagates, and by including the effect of attenuation, we write the following generalized time dependent differential equation for the E_z :

$$\frac{\partial E_z}{\partial z} + \frac{1}{v_g} \frac{\partial E_z}{\partial t} = -\frac{I \langle e^{-i\psi} \rangle}{v_g w U' / E_z^2} \left(\frac{\sin(k_y \Delta y / 2)}{k_y \Delta y / 2} \right) - \alpha E_z. \quad (10)$$

Here, α represents the attenuation coefficient of the surface wave. The detailed calculations for α are discussed in Appendix A.

Now, we discuss the longitudinal dynamics of the electron beam. We neglect the transverse motion of the electrons, and write the equations for the evolution of energy and phase of i th electron respectively as:

$$\frac{\partial \gamma_i}{\partial z} + \frac{1}{v} \frac{\partial \gamma_i}{\partial t} = \frac{eE_z}{mc^2} \cos(k_y y) e^{i\psi_i} + c.c., \quad (11)$$

$$\frac{\partial \psi_i}{\partial z} + \frac{1}{v} \frac{\partial \psi_i}{\partial t} = \frac{\omega}{c\beta^3\gamma^2} \left(\frac{\gamma_i - \gamma_R}{\gamma_R} \right). \quad (12)$$

Here, $\gamma_R = 1/\sqrt{1 - v_R^2/c^2}$ is the relativistic Lorentz factor, e represents the magnitude of the electron's charge and m is mass of the electron. The subscript R is meant for the resonant particle. At resonance, the electron velocity v is equal to the phase velocity of the co-propagating evanescent surface mode along the z -axis. Note that the electromagnetic field has $\cos(k_y y)$ type variation and it has peak value at $y = 0$. Electrons will see the maximum field at $y = 0$ while propagating along the z -direction. For the parameters of CFEL discussed earlier, the space charge field do not have any significant effect on the dynamics of the electron beam [6], and we have therefore neglected it in our calculations. Equations (10-12) can be expressed in more elegant form by defining the following dimensionless variables [6, 14]:

$$\xi = z/L, \quad (13)$$

$$\tau = \left(t - \frac{z}{v_R} \right) \left(\frac{1}{v_g} - \frac{1}{v_R} \right)^{-1} \frac{1}{L}, \quad (14)$$

$$\eta_i = \frac{k_z L}{\beta^2 \gamma^3} (\gamma_i - \gamma_R), \quad (15)$$

$$\mathcal{E} = \frac{4\pi k_z L^2}{I_A Z_0 \beta^2 \gamma^3} E_z, \quad (16)$$

$$\mathcal{J} = 4\pi \frac{k_z L^3}{Z_0 \beta^2 \gamma^3} \frac{I}{I_A} \frac{E_z^2}{v_g w U'} \left(\frac{\sin(k_y \Delta y / 2)}{k_y \Delta y / 2} \right). \quad (17)$$

Here, ξ is the dimensionless distance, which varies from 0 to 1, and τ is the dimensionless time variable, having an offset of z/v_R from the real time t , \mathcal{E} is the dimensionless surface mode field, and the normalised energy detuning of the i th electron is η_i . The dimensionless beam current is written as \mathcal{J} , $Z_0 = 1/\epsilon_0 c = 377 \Omega$ is the characteristic impedance of the free space,

and $I_A=4\pi\epsilon_0mc^3/e=17.04$ kA is the Alfvén current. With these dimensionless variables, the set of Eqs. (10-12) assume the following form:

$$\frac{\partial \mathcal{E}}{\partial \xi} + \frac{\partial \mathcal{E}}{\partial \tau} = -\mathcal{J}\langle e^{-i\psi} \rangle - \alpha L \mathcal{E}, \quad (18)$$

$$\frac{\partial \eta_i}{\partial \xi} = \mathcal{E} \cos(k_y y) e^{i\psi_i} + c.c., \quad (19)$$

$$\frac{\partial \psi_i}{\partial \xi} = \eta_i. \quad (20)$$

Equations (18-20) are known as coupled Maxwell-Lorentz equations, and these equations have to be solved numerically to study the detailed behaviour of the CFEL system with side walls. In small-signal small-gain regime, these equations can be solved analytically as described in Ref. [15]. Following the approach and by neglecting the attenuation effect, we obtain the expression for the small-signal gain of a sidewall CFEL as:

$$G = 6.75 \times 10^{-2} \times 16\pi \frac{k_z L^3}{Z_0 \beta^2 \gamma^3} \frac{I}{I_A} \frac{E_z^2}{v_g w U'} \left(\frac{\sin(k_y \Delta y / 2)}{k_y \Delta y / 2} \right)^2. \quad (21)$$

The expression for U'/E_z^2 is given in Appendix in Eq. (A.12). We observe that the above expression is similar the expression for gain derived for the case of CFEL without any side wall in Ref. [6], with some notable differences. First, the term w appearing in the denominator of the above equation appears as $\Delta y_e = \sqrt{\pi\beta_p\lambda L/4}$ in the corresponding equation for the case of CFEL without any side walls. Here, w is independent of L because of waveguiding, and can be made much smaller compared to Δy_e . Next, by comparing the expression for U'/E_z^2 given by Eq. (A.12), with the corresponding equation given in Ref. [6] for the case of CFEL without any side walls, we observe that the value of U'/E_z^2 is reduced nearly by a factor of 2 due to the presence of side walls. Thus the effective mode width for the case of CFEL with side walls can be taken as $w/2$. Hence, if we choose $w = (2/5)\Delta y_e = (2/5)\sqrt{\pi\beta_p\lambda L/4}$, we expect an enhancement in gain upto a factor of 5. Finally, we observe that there is a term containing square of a sinc function on the right side of Eq. (21). This term is maximum if $\Delta y \rightarrow 0$, which means that if all the electrons are at $y = 0$, they observe the peak of the electric field amplitude, and the gain is maximum. Taking the effect of attenuation, there will be a single pass loss $(1 - e^{-2\alpha L})$ in addition to the gain given by Eq. (21).

In the small-signal, high-gain regime, we have solved coupled Maxwell-Lorentz equations by using the collective variables as described in Ref. [6], and find the growth rate of a CFEL in side wall configuration as:

$$\mu = \frac{\sqrt{3}}{2L} \left[4\pi \frac{k_z L^3}{Z_0 \beta^2 \gamma^3} \frac{I}{I_A} \frac{E_z^2}{v_g w U'} \left(\frac{\sin(k_y \Delta y / 2)}{k_y \Delta y / 2} \right)^2 \right]^{1/3}. \quad (22)$$

Due to the effect of attenuation, the net growth rate becomes $\mu - \alpha$.

In our calculations, we have assumed that the metallic base and metallic side walls are made up of silver metal, and to minimize the effect of ohmic losses, we have kept the metallic part at the boiling point temperature of liquid nitrogen at 77 K. The attenuation effect due to dielectric loss is quite insignificant for the sapphire dielectric ($\tan \delta \leq 10^{-4}$) [7, 16], and we have neglected it in our calculations. At 77 K, for the parameters discussed earlier in the section, the ohmic attenuation coefficient as calculated by using Eq. (A.15) comes out to be 1.07 per m. This results in the single pass loss (in power) of 10.2 %. We have kept the sidewall spacing as $w = (2/5) \sqrt{\pi \beta_p \lambda L / 4} = 2.7$ mm, and considered electron beam size $\Delta y = 1.35$ mm. Taking the ohmic loss into account, we obtain the net small-signal gain as 185 % and net growth rate of about 32.4 per m for the system.

C. Numerical simulations

To study the saturation behaviour of the system, we have solved the coupled Maxwell-Lorentz equations numerically by writing a computer code using the Leapfrog method. In the numerical simulations, we have considered a total 2^{18} electrons propagating at height h . To study the effect of overlap between the electron beam and the surface mode, we have distributed electrons into 2^5 arrays along the (y, z) plane, where each array consists of 2^{13} monoenergetic electrons which are propagating along the z -direction. All electrons in one array will see the same magnitude of the electric field, depending upon the array position along the y -direction. The energy and phase of electrons will evolve in accordance of Eqs. (19) and (20), respectively. In each array, the electron beam is initialised in the phase space by using the quiet start scheme. In the quiet start scheme, electrons are assumed to have a uniform distribution in the phase space with phase of i th electron is set to be $2\pi i / N$, where N is the total number of electrons in an array.

The main parameters used in the simulations have been listed in Table 1. In Fig. 3,

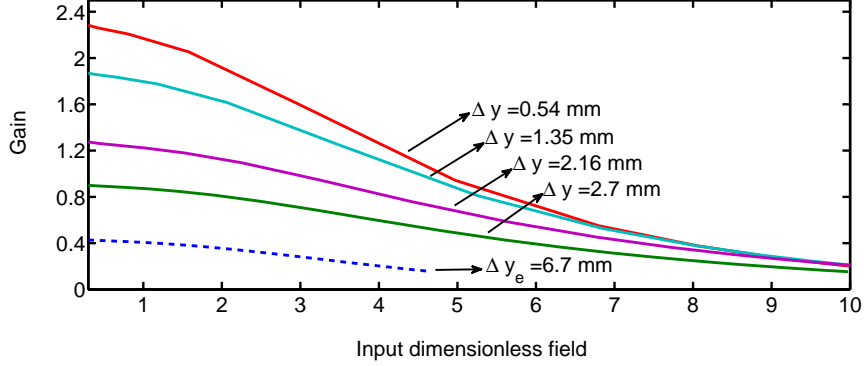


FIG. 3. Plot of net gain as a function of input electric field in CFEL oscillator. Dashed curve shows gain plot for a CFEL without side walls, and solid curves represent the case of sidewall CFEL having sidewall spacing $w=2.7$ mm.

gain has been plotted as a function of input field for different values of electron beam width. The dashed curve shows gain of a CFEL without any side walls, and solid curves represent gain of a side wall CFEL with different values of electron beam width Δy . The values of small signal gain obtained by using numerical simulations are in well agreement with the analytical results evaluated by using Eq. (21), and these results have been summarized in Table 2.

The sidewall configuration of CFEL has much improved gain as compare to the CFEL without any side walls. In the case of sidewall configuration, decrease in electron beam width results in peaking of the gain.

The CFEL system discussed here is a low gain system, and to achieve saturation, the device has to be operated in the oscillator configuration. For this purpose, a set of mirrors

TABLE II. Comparison of analytical and simulation results for net small-signal gain of CFEL.

| Electron beam width | Analytically calculated gain | Simulation results for gain |
|---------------------|------------------------------|-----------------------------|
| 6.70 mm | 43.3 % | 43.2 % |
| 2.70 mm | 87.4 % | 90.0 % |
| 2.16 mm | 127.7 % | 127.5 % |
| 1.35 mm | 185.0 % | 187.0 % |
| 0.54 mm | 223.0 % | 228.4 % |

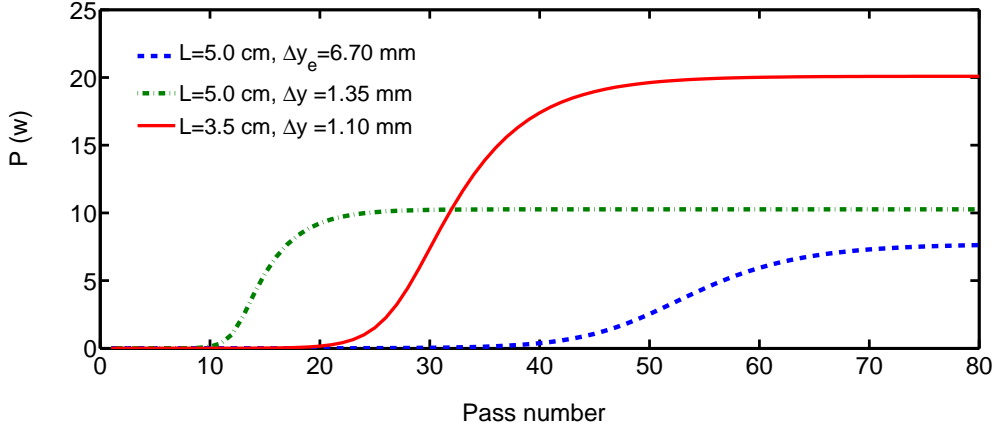


FIG. 4. Plot of power in the surface mode as a function of pass number. The dashed curve represents the case of CFEL without side walls. The dot-dashed and solid curve represent the power of a side wall CFEL with $L = 5$ cm and $L = 3.5$ cm, respectively.

are used to provide an external feedback. One mirror is assumed to have 100 % reflectivity for field amplitude, while the second mirror is having the reflectivity of field amplitude as 98 %. The electromagnetic radiation can be out coupled through the second mirror, and the output THz radiation can be guided via suitable optical arrangements to the nearby experimental station. In this configuration, the electromagnetic field reflected at the end of one pass becomes input field for the next pass. The coupled Maxwell-equations have been solved for the oscillator configuration to obtain the power in the surface mode. Figure 4 shows power as a function of pass number. For interaction length $L = 5$ cm, the sidewall CFEL as compared to a CFEL without side walls, saturates early, at around 35th pass, with a saturated power of 10.3 W; which is higher compared to the case of without side walls. Input power of the electron beam is 1932 W, and efficiency of system comes out to be 0.53 %. A rough estimate for the upper bound of the efficiency of a CFEL system can be given by [2]

$$\eta = \frac{\beta^3 \gamma^3}{(\gamma - 1)} \frac{\lambda}{L}. \quad (23)$$

The above formula is valid in the absence of heat loss due to attenuation. Including the effect of heat loss, there will be a multiplication factor of $(1 - R^2)/((1 - R^2) + (1 - e^{-4\alpha L}))$ in Eq. (23). Here, $R = 0.98$ is the reflection coefficient of the out-coupling mirror. For the prescribed parameters, we find an upper bound of 0.92 % of efficiency, which is in agreement

with the results our numerical simulations.

Next, we would like to discuss that in case of guided CFELs, we can take shorter interaction length to improve the performance of the system. As mentioned earlier, by taking the smaller beam size Δy , one can achieve higher value of gain, however, the condition on the electron beam emittance becomes stringent at smaller beam size [7, 17]. In order to maintain a given value of electron beam size Δy over the interaction length L , we require that the normalized beam emittance should satisfy $\epsilon_y \leq \beta\gamma\Delta y^2/16L$ [7]. Similar condition can be written with subscript x in the x -direction. For $L = 5$ cm, we have taken $\Delta y = w/2 = 1.3$ mm, and $\Delta x = 200\mu\text{m}$, which require a flat beam with fine beam emittances $\epsilon_y \leq 1 \times 10^{-6}$ m-rad, and $\epsilon_x \leq 2.3 \times 10^{-8}$ m-rad. Hence, to drive the CFEL system, we require an asymmetric electron beam with transverse emittance ratio $\epsilon_y/\epsilon_x \sim 45$. Such electron beams were produced only recently by employing a round to flat beam transformation to the initial round beam, as discussed in Refs. [18, 19]. The stringent requirements on the beam emittances can be relaxed by taking a small interaction length L . The additional advantage is that we can achieve high efficiency at small L , as clear from Eq. (23). It has to be noted that with decrease in L , the gain will decrease, and one has to optimize L such that the system can overcome the losses. This criteria can be easily achieved in sidewall CFEL, which has improved gain as compare to the CFEL without side walls. We take $L=3.5$ cm for a sidewall CFEL, for which the net small signal gain is 69 %, and we require an electron beam with relaxed transverse emittance ratio of 31. In Fig. 4, the solid curve shows the power in the surface mode for a sidewall CFEL with $L = 3.5$ cm. As expected, CFEL at shorter interaction length saturates at higher power of about 20.1 W, and has an increased efficiency of 1 %. Analysis in linear as well as in the non-linear regime shows that the guiding of surface mode in CFEL system is helpful in improving performance of the system.

III. DISCUSSIONS AND CONCLUSIONS

In this paper, we have presented a theory of waveguided Čerenkov FEL in the single slab geometry, where the waveguiding is provided by metallic side walls. The waveguiding is particularly useful to enhance the performance of a CFEL at longer wavelength, where diffraction effects are prominent and reduce the gain. Due to waveguiding, the mode width can be taken much smaller compared to what can be achieved in the case of freely prop-

agating mode. This approach has been used earlier for undulator based FELs, as well as Smith-Purcell FELs [10–12], and in this paper, we have extended this approach for CFELs.

Our analysis is built on the model discussed earlier in the Refs. [6, 13]. We have set coupled Maxwell-Lorentz equations for the system. These equations have been solved analytically to obtain small-signal gain and growth rate of the system. In the non-linear regime, we solved these equations numerically by using Leapfrog method to obtain the output power at saturation. We find that a CFEL with length $L = 3.5$ cm, spacing between side wall 2.2 mm, can be operated at 0.11 THz by using a 56 keV, 35 mA electron beam to give output power of tens of watt with an efficiency of 1 % at saturation. We also checked that the requirements on the electron beam emittance for the required electron beam width are not stringent.

We want to emphasize that in Ref. [6], we performed the analysis of CFEL having no side walls, by analysing the singularity in the reflectivity of the dielectric slab (placed on a conducting surface) for the incident evanescent wave, and deriving the expressions for the parameters χ and χ_1 . The growth of surface mode is understood in terms of χ parameter, and the space charge effect is studied by using the parameter χ_1 . In Refs. [6, 14], it has been shown that the above mentioned approach, and the approach followed by Levush *et al.* [13], which is also adopted in the present paper; give same result for the case of CFELs, and SP-FELs having no side walls. We have checked that even in the presence of side walls, the χ and χ_1 parameters can be derived and analysis can be performed in terms of these parameters, and it gives the same results as described in this paper. The same criteria will be applicable in the SP-FELs [14, 20], and the approach based on Maxwell-Lorentz equations can certainly be extended to the case of sidewall SP-FELs. We would like to mention that our analysis can also be extended to study the CFEL based on negative refractive index material. CFEL based on negative index material will work like a BWO [9], and can be studied by following the analysis given in Refs. [14, 17].

To conclude, we have proposed a CFEL with metallic side walls. A detailed analysis for the guided surface mode is presented. Realistic effects such as effects due to transverse variation of the field, and attenuation effects have been included in the analysis. Our analysis shows that a side wall CFEL has much improved gain as compared to CFEL without side walls, and can give significant output power in THz regime, even after including the attenuation effects. The presented analysis can be very useful to design a practical CFEL

device with side walls.

Appendix A: POWER, GROUP VELOCITY AND ATTENUATION-COEFFICIENT OF THE SURFACE MODE SUPPORTED IN A SIDE WALL ČERENKOV FEL

In this Appendix, we have evaluated power and group velocity of the surface mode supported in a sidewall Čerenkov FEL. The obtained results are then used to calculate the attenuation coefficient of the surface mode due to loss present in the system. The schematic of a side wall CFEL is shown in Fig. 1, where the metallic sidewalls are placed at $y = \pm w/2$. The electromagnetic surface mode supported by this structure can be obtained by combining two plane waves, each having frequency ω and wave vector $k_0 = \sqrt{k_y^2 + k_z^2}$, travelling in different directions in the (y, z) plane. The dielectric slab is an isotropic structure in the (y, z) plane, and the optical properties of the system will remain invariant under any arbitrary rotation in the (y, z) plane. By using the property of isotropy in the results derived earlier for a CFEL without any side walls [6], we obtain the electromagnetic field components of the surface mode in the vacuum region of a sidewall CFEL as:

$$H_y^I = (k_z H / k_0) \cos(k_y y) e^{i(k_z z - \omega t)} e^{-\Gamma(x-h)} + \text{c.c.}, \quad (\text{A1})$$

$$H_z^I = (-i k_y H / k_0) \sin(k_y y) e^{i(k_z z - \omega t)} e^{-\Gamma(x-h)} + \text{c.c.}, \quad (\text{A2})$$

$$E_x^I = (k_0 H / \epsilon_0 \omega) \cos(k_y y) e^{i(k_z z - \omega t)} e^{-\Gamma(x-h)} + \text{c.c.}, \quad (\text{A3})$$

$$E_y^I = (k_y \Gamma H / \epsilon_0 \omega k_0) \sin(k_y y) e^{i(k_z z - \omega t)} e^{-\Gamma(x-h)} + \text{c.c.}, \quad (\text{A4})$$

$$E_z^I = (-i k_z \Gamma H / \epsilon_0 \omega k_0) \cos(k_y y) e^{i(k_z z - \omega t)} e^{-\Gamma(x-h)} + \text{c.c.}, \quad (\text{A5})$$

and $H_x^I = 0$. Inside the dielectric medium, the components of electromagnetic field are given by

$$H_y^{II} = \frac{\epsilon k_z \Gamma H \cos[k_1(x+d)]}{k_1 k_0 \sin(k_1 d)} \cos(k_y y) e^{\Gamma h} e^{i(k_z z - \omega t)} + \text{c.c.}, \quad (\text{A6})$$

$$H_z^{II} = \frac{-i \epsilon k_y \Gamma H \cos[k_1(x+d)]}{k_1 k_0 \sin(k_1 d)} \sin(k_y y) e^{\Gamma h} e^{i(k_z z - \omega t)} + \text{c.c.}, \quad (\text{A7})$$

$$E_x^{II} = \frac{k_0 \Gamma H \cos[k_1(x+d)]}{\epsilon_0 \omega k_1 \sin(k_1 d)} \cos(k_y y) e^{\Gamma h} e^{i(k_z z - \omega t)} + \text{c.c.}, \quad (\text{A8})$$

$$E_y^{II} = \frac{k_y \Gamma H \sin[k_1(x+d)]}{\epsilon_0 \omega k_0 \sin(k_1 d)} \sin(k_y y) e^{\Gamma h} e^{i(k_z z - \omega t)} + \text{c.c.}, \quad (\text{A9})$$

$$E_z^{II} = \frac{-ik_z \Gamma H \sin[k_1(x+d)]}{\epsilon_0 \omega k_0 \sin(k_1 d)} \cos(k_y y) e^{\Gamma h} e^{i(k_z z - \omega t)} + \text{c.c.} \quad (\text{A10})$$

Here, $H_x^{II} = 0$ and $k_1 = \sqrt{\epsilon \omega^2 / c^2 - k_y^2 - k_z^2}$. Power flow in the surface mode can be evaluated by integrating the Poynting vector over x in the range $(0, \infty)$, and over y in the range $(-w/2, w/2)$. Total power in the surface mode is sum of power flow in the vacuum and inside the dielectric medium, which we obtain as:

$$P = \frac{w \gamma_p k_z Z_0}{2 \beta_p k_0^2} \left[1 + \frac{1}{\epsilon^2 a^2} + \frac{k_0 d (1 + a^2)}{\epsilon \gamma_p a^2} \right] H^2 e^{2\Gamma h}. \quad (\text{A11})$$

Here, $\beta_p = \omega / ck_0$ is the phase velocity of the surface mode in unit of c , $\gamma_p = 1 / \sqrt{1 - \beta_p^2}$, and $a = (\gamma_p / \epsilon) \sqrt{\epsilon \beta_p^2 - 1}$. It should be noted that the total power in a side wall CFEL is $k_z / 2k_0$ times the power contained in the surface mode supported in CFEL without any side walls [6]. This is obvious as the electromagnetic fields in a sidewall CFEL are propagating at angle, whose cosine gives the factor k_z / k_0 , with respect to the z -direction. The factor $1/2$ accounts for the variation of electromagnetic fields along the y -direction. The energy stored in fields is obtained by integrating the energy density over the volume of dielectric and the vacuum region as:

$$\frac{U'}{E_z^2} = \frac{k_0 \gamma_p^3}{2ck_z^2 Z_0} \left[1 + \frac{1}{\epsilon^2 a^2} + \frac{k_0 d \beta_p^2 (1 + a^2)}{\gamma_p a^2} \right] e^{2\Gamma h}. \quad (\text{A12})$$

Note that above result has been expressed in term of peak field amplitude E_z at the location of electron beam by using Eq. (A5). The energy velocity of the electromagnetic fields is given by PL/U . For a Čerenkov FEL, the energy velocity is equal to the group velocity [6]. Using Eqs. (A11) and (A12), we obtain the group velocity of the surface mode supported in a side wall CFEL as:

$$v_g = \frac{\beta_p ck_z}{k_0} \frac{[\beta_p^2 \gamma_p^3 (\epsilon - 1) + k_0 d \epsilon (1 + a^2)]}{[\beta_p^2 \gamma_p^3 (\epsilon - 1) + k_0 d \epsilon^2 \beta_p^2 (1 + a^2)]}. \quad (\text{A13})$$

In a sidewall CFEL, the group velocity of the surface mode is k_z / k_0 times the group velocity of a CFEL without any sidewalls [6].

Next, we evaluate the attenuation coefficient of the surface mode, which is given by [21]

$$\alpha^{m,d} = \frac{P_l^{m,d}}{2P}, \quad (\text{A14})$$

where P_l represents the power loss per unit length along the z -direction, and the subscripts m and d are used to represent the metallic conductor and dielectric medium respectively.

In a metallic structure with finite conductivity Σ , dissipation of power occurs due to the ohmic losses. At the location $x = -d$, the power loss per unit length along the surface of metal is given by: $(R_s/2) \int_{-w/2}^{w/2} |H_y^{II}|^2 dy$ [22], where $R_s = \sqrt{\mu_0 \omega / 2 \Sigma}$ is surface resistance of the metal. At the location of side walls $y = \pm w/2$, we can write power loss per unit length as: $(R_s/2) (\int_{-d}^0 |H_z^{II}|^2 dx + \int_0^\infty |H_z^I|^2 dx)$ [22]. The total power dissipated along the metallic surface P_l^m is sum of power dissipated at $x = -d$, and the power dissipated at the side walls. By performing the required algebra for P_l^m and by using the expression (A14), we obtain the ohmic attenuation coefficient as:

$$\alpha^m = \frac{2\beta_p R_s k_y^2 [1 + (w\Gamma k_z^2 / 2a^2 k_y^2)(1 + a^2) + (\epsilon^2 \Gamma^3 / k_1^3)(a + k_1 d(1 + a^2))]}{\gamma_p w k_z \Gamma Z_0 [1 + (1/\epsilon^2 a^2) + (k_0 d / \epsilon \gamma_p a^2)(1 + a^2)]}. \quad (\text{A15})$$

Inside the dielectric medium, losses are described in the terms of complex relative permittivity $\tilde{\epsilon} = \epsilon - i\epsilon''$ with tangent loss defined as $\tan \delta = \epsilon'' / \epsilon$ [23]. Now, the power loss per unit length inside the dielectric material is given by $P_l^d = \epsilon_0 \epsilon \omega \tan \delta \int_{-d}^0 \int_{-w/2}^{w/2} (|E_x^{II}|^2 + |E_y^{II}|^2 + |E_z^{II}|^2) dx dy$. By using Eqs. (A8-A10), we first evaluate P_l^d , and then by using Eq. (A14), we obtain the attenuation coefficient α^d as:

$$\alpha^d = \frac{k_0^2 \tan \delta [\gamma_p (2 - \epsilon \beta_p^2) + \epsilon^2 \beta_p^2 k_0 d (1 + a^2)]}{2k_z [\gamma_p (1 + \epsilon^2 a^2) + \epsilon k_0 d (1 + a^2)]}. \quad (\text{A16})$$

Total attenuation coefficient α of the surface wave can be written as $\alpha = \alpha^m + \alpha^d$, which gives attenuation due to both ohmic loss and due to the loss present in the dielectric structure.

ACKNOWLEDGMENT

We acknowledge Professor P. D. Gupta and Professor S. B. Roy for constant encouragement. One of us (YK) gratefully acknowledges Homi Bhabha National Institute, Department of Atomic Energy (India) for financial support during the work.

-
- [1] P. H. Siegel, IEEE Trans. Microwave Theory Tech. **50**, 910 (2002).
 - [2] J. E. Walsh and J. B. Murphy, IEEE J. Quantum Electron. **18**, 1259 (1982).
 - [3] J. Walsh, B. Johnson, G. Dattoli, and A. Renieri, Phys. Rev. Lett. **53**, 779 (1984).
 - [4] I. J. Owens and J. H. Brownell, Phys. Rev. E **67**, 036611 (2003).

- [5] H. L. Andrews and C. A. Brau, *J. Appl. Phys.* **101**, 104904 (2007).
- [6] Y. Kalkal and V. Kumar, *Phys. Rev. ST Accel. Beams* **18**, 030707 (2015).
- [7] Y. Kalkal and V. Kumar, (to be published).
- [8] I. J. Owens and J. H. Brownell, *J. Appl. Phys.* **97**, 104915 (2005).
- [9] D. Li, Y. Wang, M. Hangyo, Y. Wei, Z. Yang, and S. Miyamoto, *Appl. Phys. Lett.* **104**, 194102 (2014).
- [10] D. Li, K. Imasaki, X. Gao, Z. Yang, and G.-S. Park, *Appl. Phys. Lett.* **91**, 221506 (2007).
- [11] H. L. Andrews, J. D. Jarvis, and C. A. Brau, *J. Appl. Phys.* **105**, 024904 (2009).
- [12] J. T. Donohue and J. Gardelle, *Phys. Rev. ST Accel. Beams* **14**, 060709 (2011).
- [13] B. Levush, T. M. Antonsen, A. Bromborsky, W. R. Lou, and Y. Carmel, *IEEE Trans. Plasma Sci.* **20**, 263 (1992).
- [14] V. Kumar and K.-J. Kim, *Phys. Rev. E* **73**, 026501 (2006).
- [15] C. A. Brau, *Free-electron laser* (Academic Press, San Diego, 1990).
- [16] W. Westphal and A. Sils, Tech. Rep. AFML-TR-72-39, Massachusetts Institute of Technology (1972).
- [17] K.-J. Kim and V. Kumar, *Phys. Rev. ST Accel. Beams* **10**, 080702 (2007).
- [18] P. Piot, Y.-E. Sun, and K.-J. Kim, *Phys. Rev. ST Accel. Beams* **9**, 031001 (2006).
- [19] J. Zhu, P. Piot, D. Mihalcea, and C. R. Prokop, *Phys. Rev. ST Accel. Beams* **17**, 084401 (2014).
- [20] V. Kumar and K.-J. Kim, in *Proceedings of FEL05* (2005), pp. 274–277.
- [21] S. Y. Liao, *Microwave Devices and Circuits* (Dorling Kindersley, India, 2011).
- [22] J. D. Jackson, *Classical Electrodynamics* (John Wiley, Singapore, 1999).
- [23] R. A. Waldron, *Theory of guided electromagnetic waves* (London ; New York : Van Nostrand Reinhold, 1970).